Automatic Navigation of a Microrobotic Swarm for Tracking Multiple Mobile Targets

Qian Zou, *Graduate Student Member, IEEE*, Xingjian Liu, *Member, IEEE*, and Jiangfan Yu, *Member, IEEE*

***Abstract*—Microrobotic swarms actuated by magnetic fields have attracted considerable attention in the field of automatic control. Developing effective control schemes for microrobotic swarms to track multiple mobile targets is still a major challenge. In this work, we propose an optimized rapidly-exploring random tree star (ORRT*) algorithm to generate desired paths connecting the swarm and the targets. A path selection strategy is developed to select the shortest path, and subsequently the immediate target to track is determined. The sliding mode (SM) motion controller is then presented to achieve the tracking of multiple mobile targets using microrobotic swarms. Comparisons are performed to validate the effectiveness of the control scheme, including the path planner and the motion controller. Finally, simulations and experiments of tracking multiple mobile targets in a virtual micromaze are conducted.**

***Index Terms*—Swarm control, path planning, tracking multiple mobile targets.**

I. Introduction

UNTETHERED milli/microrobots have attracted extensive attention due to their potential applications in various biomedical operations, e.g., untethered manipulation in poorly accessible space, in-body drug delivery, controllable drug administration and local therapy in the GI tract [1], [2], [3], [4], [5], [6], [7], [8], [9]. In particular, milli/microrobots exhibit great capabilities to perform tasks in hard-to-reach and narrow regions in a living body due to their outperforming mobility and flexible maneuverability [10], [11]. To date, different microrobots have been investigated, such as, a jellyfish-inspired millirobot [12], an amphibious origami millirobot [13], and a functional soft microrobot with p-Si doping [14]. Microrobotic swarms can serve as promising candidates for large-volume targeted cargo delivery and imaging resolution enhancement [15], [16]. Unlike centimeter-scale robots, microrobotic swarms can hardly be equipped with on-board sensors and actuators for individual motion control. External power sources are critical to actuate the motion of microrobotic swarms, such as optical [17], acoustic [18], electric [19], [20] and magnetic fields [21], [22]. Chemical fuels can also serve for the same purpose in some cases [23], [24]. Compared to other power sources, magnetic fields are widely used to actuate microrobotic swarms due to their advantages, e.g., ability to penetrate deep tissues [25], biocompatibility to living organisms [26], and easy implementation of actuation systems [27]. In order to realize the desired swarm behaviors, regulating input magnetic fields to control the swarming agents is important. In some cases, microrobotic swarms are required to move from the initial position to the targeted static position, such as, delivering targeted drugs to tumor site. During the movement, they are demanded to follow the planned path to avoid collision with obstacles and solid walls. Swarms can be used to track single or multiple mobile targets, e.g., to track and capture bacteria for antimicrobial applications. Moreover, the optimal control of swarms to track multiple mobile targets is also fundamentally challenging but attractive.

Generating desired paths and selecting the optimal path are prerequisites for the tracking of multiple mobile targets. To date, path planning algorithms for tracking static targets using microrobots have been extensively studied, such as, a rapidly-exploring random tree (RRT) path planner for a two-microrobot system [28], an RRT-GoalZoom path generator for soft untethered grippers [29] and a grasping motion planner for an untethered magnetic microgripper [30]. Since the positions of multiple mobile targets keep changing, efficient path planning algorithms with path selection strategy need to be further developed.

Motion control of swarms by regulating the magnetic field parameters shall be achieved for the precise control of swarm moving direction and velocity. Although various motion control methods of milli/microrobots have been broadly reported, e.g., an independent control strategy of multiple millirobots is proposed for position control and path following [31], an image-based visual servoing control method of helical microswimmers is presented for planar path following [32], a learning-based servo control strategy of helical microrobots is proposed for locomotion control [33], a visual feedback path-following controller of needle-like microrobots is developed for multimodal

Manuscript received 6 September 2022; accepted 16 January 2023. Date of publication 2 February 2023; date of current version 12 September 2024. This letter was recommended for publication by Associate Editor J. Liu and Editor X. Liu upon evaluation of the reviewers' comments. This work was supported in part by the National Key R&D Program of China under Project 2022YFA1207100, in part by the National Natural Science Foundation of China under Project 62103347, in part by Guangdong Basic and Applied Basic Research Foundation under Project 2022A1515110499, and in part by the Shenzhen Institute of Artificial Intelligence and Robotics for Society under Project AC01202201007-03. *(Corresponding author: Jiangfan Yu.)*

Qian Zou is with the School of Science and Engineering, The Chinese University of Hong Kong, Shenzhen 518172, China (e-mail: qianzou@link.cuhk.edu.cn).

Xingjian Liu is with the School of Mechanical Engineering, Dalian University of Technology, Dalian 116024, China (e-mail: xjliu@dlut.edu.cn).

Jiangfan Yu is with the School of Science and Engineering, and School of Medicine, The Chinese University of Hong Kong, Shenzhen 518172, China, and also with the Shenzhen Institute of Artificial Intelligence and Robotics for Society, Shenzhen 518129, China (e-mail: yujiangfan@cuhk.edu.cn).

This letter has supplementary downloadable material available at https://doi.org/10.1109/LRA.2023.3241813, provided by the authors.

Digital Object Identifier 10.1109/LRA.2023.3241813

2377-3766 © 2023 IEEE. Personal use is permitted, but republication/redistribution requires IEEE permission.
See https://www.ieee.org/publications/rights/index.html for more information.

Authorized licensed use limited to: The University of Osaka. Downloaded on April 23,2025 at 01:57:31 UTC from IEEE Xplore. Restrictions apply.

locomotion control [34], and a LQR controller of a helical microswimmer is proposed for direction control [35], the automatic control of microrobotic swarms is still challenging. The complex interactions among the swarm agents are significantly affected by the external magnetic fields and ambient environments. Therefore, to guarantee the swarm stability, which indicates that the swarm can maintain its ribbon-like pattern when following the planned path, is challenging. Meanwhile, the precise analytical model of the swarm is hard to obtain [36]. Effective control schemes for the moving direction and velocity of the swarm are still under investigation.

Motivated by the aforementioned issues in path planning and swarm motion control, an effective and efficient control scheme is proposed to achieve collision-free automatic navigation of a microswarm to track multiple mobile targets with a path selection strategy. The desired paths are generated by an optimal rapidly-exploring random tree star (ORRT*) path planner. The path selection strategy then chooses the shortest path and subsequently the immediate target is determined at each moment. The moving direction and velocity of the swarm is controlled by a sliding mode (SM) motion controller to achieve high tracking precision. In order to validate the effectiveness of the control scheme, the ORRT* path planner and the SM motion controller are compared separately with the RRT* path planner and the PID motion controller. Simulations and experiments of tracking multiple mobile targets are also performed.

II. Control Scheme

A. Path Planning Algorithm

In order to generate the desired path, an optimized rapidly-exploring random tree star (ORRT*) algorithm is proposed and its schematics is demonstrated in Fig. 1. Taking the starting point (i.e., node ξ_s) as the root node, a random node ξ_{rand} is sampled from the obstacle-free space. According to Algorithm 1, the **NearestNode** function will then check the nearest node of the randomly sampled node ξ_{rand}, i.e., node ξ_{near}, and it is added to the tree as the current new node ξ_{new} by the **Steer** function. The ORRT* algorithm then uses the **CollisionCheck** function in Algorithm 1 to check whether there is any collision between the branch $\xi_s\,\xi_{new}$ and the walls of the micromaze. In order to avoid collision between the swarm and the walls taking the physical size of the swarm into consideration, the collision buffer layers (i.e., the blue regions in Fig. 1) are added surrounding the walls. The thickness of the collision buffer layer σ_h is determined by the length of the detected swarm at each moment and it is expressed as:

$$\sigma_h = c_h \frac{l_s^t}{2} \tag{1}$$

where l_s^t is the length of the detected swarm at moment t and c_h is a constant ranging from 1.5 to 2, which is used to compensate the detection error. If there is no collision between the swarm and the walls of the micromaze, the next step is to generate a neighboring area by the **NearArea** function, whose center is the current node ξ_{new}. The **ChooseParent** and **Rewire** functions in Algorithm 1 then search the best node ξ_{best} in the neighboring area, indicating that the path length from the starting node ξ_s to the best node ξ_{best} is the shortest. Once the tree nodes reach the goal point (i.e., node ξ_g), the initial path is obtained, which is shown in Fig. 1(a). It is then optimized

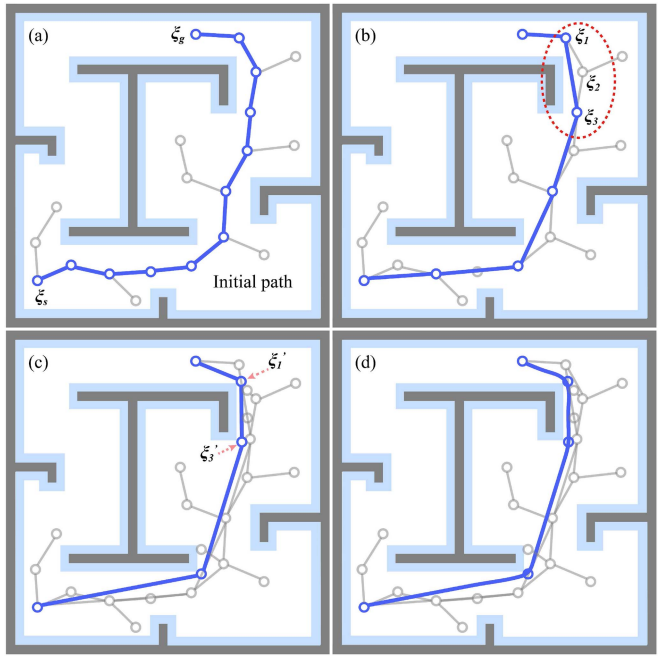

Fig. 1. The schematics of the ORRT* path planning algorithm. (a) Initial path generation. ξ_s and ξ_g are the starting and goal points. (b) Path optimization by the **TriangleInequality** function in Algorithm 1. ξ_1, ξ_2 and ξ_3 form a triangle. (c) Path optimization by the **BiasedSampling** and **TriangleInequality** functions in Algorithm 1. ξ_1' and ξ_3' are the nodes generated by the **BiasedSampling** function. (d) Path smoothing by the **Smoothing** function in Algorithm 1. The blue circles are the effective tree nodes and the blue lines denote the effective branches of the tree. The gray circles and gray lines are not used to build the path connecting the starting and goal points.

Algorithm 1: ORRT* Algorithm.

CollisionBufferLayer();
$T \leftarrow InitTree()$;
$T \leftarrow InsertNode(\xi_s, T)$;
for $k = 1$ **to** K **do:**
  $\xi_{rand} \leftarrow Sample(k)$;
  $\xi_{near} \leftarrow Nearest(\xi_{rand}, T)$;
  $\xi_{new} \leftarrow Steer(\xi_{rand}, \xi_{near})$;
  if$(CollisionCheck(\xi_{near}, \xi_{new})$ **then:**
    $\xi_{na} \leftarrow NearArea(\xi_{new}, T, r)$;
    $\xi_{best} \leftarrow ChooseParent(\xi_{na}, \xi_{near}, \xi_{new})$;
    $T \leftarrow InsertNode(\xi_{best}, \xi_{new}, T)$;
    $T \leftarrow Rewire(\xi_{na}, \xi_{best}, \xi_{new}, T)$;
    if$(PathFound$ **then:**
      $T_t \leftarrow TriangleInequality(\xi_s, \xi_g, T)$;
      $T_b \leftarrow BiasedSampling(\xi_s, \xi_g, T_t)$;
      $T_i \leftarrow TriangleInequality(\xi_s, \xi_g, T_b)$;
      $T_f \leftarrow Smoothing(\xi_s, \xi_g, T_i)$;
return T_f

Authorized licensed use limited to: The University of Osaka. Downloaded on April 23,2025 at 01:57:31 UTC from IEEE Xplore. Restrictions apply.

by the **TriangleInequality** function in Algorithm 1, and the mathematical formula is represented by [37]:

$$a + b \geq c \tag{2}$$

where a, b are the lengths of two sides of a triangle and c is the length of the remaining side. As shown in the red dotted area of Fig. 1(b), in the triangle $\Delta\xi_1\xi_2\xi_3$, the length of side $\xi_1\xi_3$ is less than to the sum of the lengths of the other two sides, i.e., side $\xi_1\xi_2$ and $\xi_2\xi_3$, which is expressed as:

$$|\overrightarrow{\xi_1\xi_3}| < |\overrightarrow{\xi_1\xi_2}| + |\overrightarrow{\xi_2\xi_3}| \tag{3}$$

The path planner then chooses side $\xi_1\xi_3$ as the new branch. Therefore, the number of tree nodes of the optimized path significantly decreases as compared with that of the initial path. To further optimize the path, the **BiasedSampling** function in Algorithm 1 generates several nodes as close as possible to the walls, as shown in Fig. 1(c). In this case, the collision buffer layer is taken into account. With these nodes, the path can be optimized if the maximum iteration is reached. In order to maintain the dynamic stability of the swarm, the path is smoothened by the **Smoothing** function in Algorithm 1 to avoid the sudden changes of the moving direction of the swarm. The smoothened path is demonstrated in Fig. 1(d).

B. Path Selection Strategy

Herein, to realize the tracking of multiple mobile targets, we propose a path selection strategy to choose the shortest path, and the immediate target to track is then picked. Its schematics is shown in Fig. 2. Since multiple targets exist, multiple paths $\rho^t_{g_i}$ are generated by the ORRT* algorithm to connect the swarm and targets. Their mathematical representation can be expressed as:

$$\begin{aligned}\rho^t_{g_i} = \{&(x^t_s, y^t_s)|t, (x^t_{i_1}, y^t_{i_1})|t, \ldots, (x^t_{i_n}, y^t_{i_n})|t, \ldots,\\ &(x^t_{i_N}, y^t_{i_N})|t, (x^t_{g_i}, y^t_{g_i})|t\}\end{aligned} \tag{4}$$

where $t \in [t_1, t_T]$, $n \in [1, N]$, $i \in [1, I]$, $(x^t_{i_n}, y^t_{i_n})$ is the n-th point of the planned path at moment t, $M^t(x^t_s, y^t_s)$ and $G^t_i(x^t_{g_i}, y^t_{g_i})$ are the positions of the swarm and the i-th target at moment t, respectively, and their lengths $\tau^t_{g_i}$ are then expressed as:

$$\begin{aligned}\tau^t_{g_i} = &\sqrt{(x^t_s - x^t_{i_1})^2 + (y^t_s - y^t_{i_1})^2} + \cdots\\ &+ \sqrt{(x^t_{i_{n-1}} - x^t_{i_n})^2 + (y^t_{i_{n-1}} - y^t_{i_n})^2} + \cdots\\ &+ \sqrt{(x^t_{i_{N-1}} - x^t_{i_N})^2 + (y^t_{i_{N-1}} - y^t_{i_N})^2}\\ &+ \sqrt{(x^t_{i_N} - x^t_{g_i})^2 + (y^t_{i_N} - y^t_{g_i})^2}\end{aligned} \tag{5}$$

When the path lengths are obtained, the path selection strategy selects the shortest path to determine the immediate target, and the mathematical representation of the selecting process can be expressed as:

$$\rho^t_s \leftarrow min\{\tau^t_{g_1}, \tau^t_{g_2}, \ldots, \tau^t_{g_i}, \ldots, \tau^t_{g_I}\} \tag{6}$$

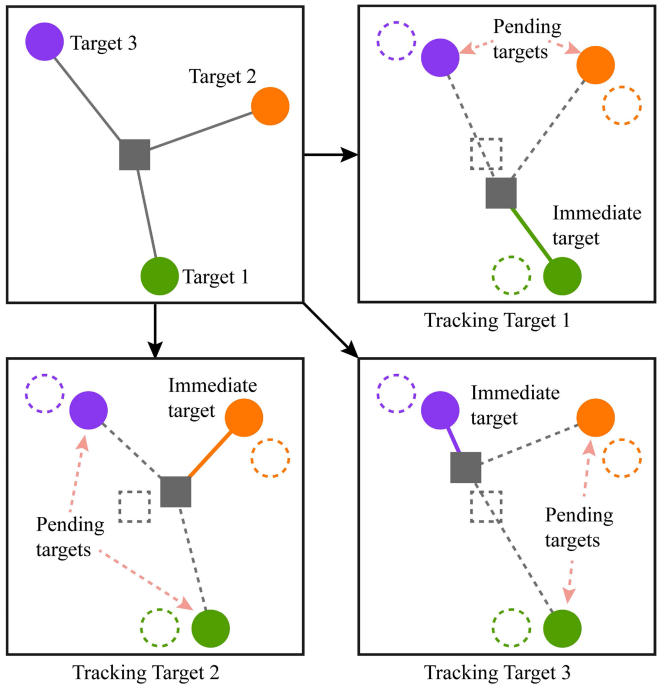

Fig. 2. The schematics of the path selection strategy. Three cases are presented, i.e., tracking Target 1, Target 2 and Target 3. The green, orange and purple circles denote the mobile targets and the black rectangle represents the swarm. The target with the shortest path is selected as the immediate target and the others are pending targets.

where ρ^t_s is the path with the shortest length. As demonstrated in Fig. 2, there are three cases. For example, if the length of the path connecting the swarm and Target 1 (i.e., the green curve) is the shortest one, Target 1 will be selected as the immediate target, and the swarm will follow the path to track Target 1 at the current moment. The other two targets, i.e., Target 2 and Target 3, are considered as the pending targets, indicating that their motion and paths are neglected by the controller until their paths become the shortest one.

C. Motion Control Algorithm

To precisely control the motion of the swarm (i.e., the moving direction and velocity of the swarm), a sliding mode (SM) motion controller is proposed. Instead of parametric equations, the planned path generated by the ORRT* algorithm is defined by a sequence of key points. Each two adjacent points are regarded as a basic segment, e.g., line segment $P_m P_{m+1}$. The target tracking is an iterative procedure, and each iteration exits when the center of the swarm is sufficiently close to the ending point of current basic segment, which is expressed as:

$$d^t_{S,P_{m+1}} < \lambda \tag{7}$$

where $d^t_{S,P_{m+1}}$ is the distance between the swarm center and the ending point of current basic segment P_{m+1} at moment t, and λ is a real constant. In this work, $\lambda = 5$ μm.

1) Sliding Mode Module: In order to achieve the precise control of swarm moving direction and velocity, the sliding mode module is proposed. When the swarm is controlled to move

Authorized licensed use limited to: The University of Osaka. Downloaded on April 23,2025 at 01:57:31 UTC from IEEE Xplore. Restrictions apply.

along the line segment P_mP_{m+1}, the distance error between the swarm position M and desired position M_d can be defined as $e = M - M_d$. The deviation of the distance error is then given as:

$$\dot{e} = \dot{M} - \dot{M}_d = c_m u \tag{8}$$

where u is the control signal of the sliding mode module and c_m is a constant calibrated by the experiments. The integral sliding surface function s can be selected as:

$$s = e + c_i \int_0^t e\, dt \tag{9}$$

where c_i is a constant of the integral component. Accordingly, the derivation of the sliding surface $\dot{s}$ can be expressed as:

$$\dot{s} = \dot{e} + c_i e \tag{10}$$

To ensure that the system states approach the sliding surface monotonically in finite steps, the reaching law is selected as:

$$\dot{s} = -\varepsilon \cdot sgn(s) - ks \tag{11}$$

where ε and k are real constants and $sgn(x)$ is the sign function, which can be expressed as:

$$sgn(x) = \begin{cases} -1, & x < 0 \\ 0, & x = 0 \\ 1, & x > 0 \end{cases} \tag{12}$$

The control law of the sliding mode module is then defined as:

$$u = \frac{-\varepsilon \cdot sgn(e + c_i \int_0^t e\, dt) - k \cdot c_i \int_0^t e\, dt - (k + c_i)e}{c_m} \tag{13}$$

The stability of the system can be analyzed by defining a Lyapunov function, which is expressed as:

$$V = \frac{1}{2}s^2 \tag{14}$$

Its deviation can be expressed as:

$$\begin{aligned} \dot{V} &= s\dot{s} \\ &= s \cdot [-\varepsilon \cdot sgn(s) - ks] \\ &= -\varepsilon \cdot sgn(s) \cdot s - ks^2 \\ &= \begin{cases} \varepsilon s - ks^2, & s < 0 \\ 0, & s = 0 \\ -\varepsilon s - ks^2, & s > 0 \end{cases} \end{aligned} \tag{15}$$

The parameter $\varepsilon > 0$ and $k > 0$, so $\dot{V} \leq 0$, and thus, the reachability condition of the sliding surface is proved. Therefore, the control signal u can be used for controlling the moving direction and velocity of the swarm.

2) Direction Control: The goal of swarm direction control is to minimize the distance error through the entire target tracking process and its schematics in an iteration is demonstrated in Fig. 3. To precisely tune the moving direction of the swarm, the direction angle α_d (i.e., the angle between the moving direction of the swarm and X axis) and the compensation angle α_c (i.e., the angle between the moving direction of the swarm and line segment P_mP_{m+1}) are introduced. As shown in **Case I** of Fig. 3,

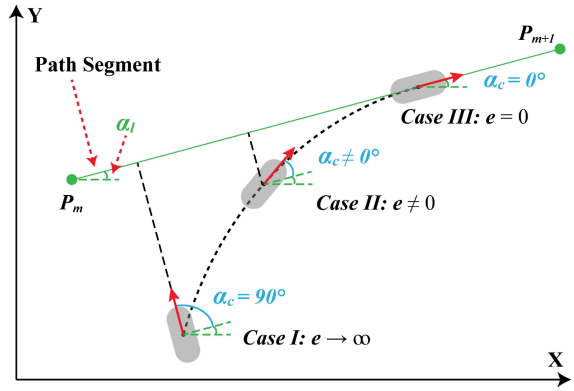

Fig. 3. The schematics of swarm moving direction control. The rounded rectangles denote the swarm. The red arrow represents the moving direction of the swarm. The angle between line segment P_mP_{m+1} and X axis is denoted by α_l.

the distance error between the swarm center and the line segment P_mP_{m+1}, i.e., e, approaches the positive infinity. In this case, the compensation angle α_c is equal to $\pi/2$ to achieve a quick converge of distance error, indicating that the moving direction of the swarm is perpendicular to the line segment P_mP_{m+1}. The direction angle of **Case I** can be expressed as:

$$\alpha_d = \alpha_l + \alpha_c = \alpha_l + \frac{\pi}{2} \tag{16}$$

where α_l is the angle between the line segment P_mP_{m+1} and X axis. In **Case II**, if the swarm is deviated from the line segment P_mP_{m+1}, the compensation angle is expressed as:

$$\alpha_c = c_d u \tag{17}$$

where c_d is a tuning constant of the direction control. A suitable compensation angle, which is determined by the distance error e, can maintain the balance between the converge speed and smooth movement of the swarm. Accordingly, the direction angle α_d can be expressed as:

$$\alpha_d = \alpha_l + \alpha_c = \alpha_l + c_d u \tag{18}$$

For **Case III**, the swarm locates on the line segment P_mP_{m+1}. The compensation angle α_c is equal to zero to remain the low distance error and the direction angle is expressed as:

$$\alpha_d = \alpha_l + \alpha_c = \alpha_l \tag{19}$$

Therefore, the moving direction of the swarm can be obtained.

3) Velocity Control: Despite of swarm direction control, the velocity control of the swarm is developed to further reduce the distance error during the locomotion of the swarm. The pitch angle of the magnetic field, which determines the velocity of the swarm, can be expressed as:

$$\gamma_v = s(c_v u, \gamma_m) \tag{20}$$

where c_v is a tuning constant of the velocity control, γ_m is the largest pitch angle that the swarm can still maintain its stability, and $s(m, n)$ is a selecting function [38], which returns

Authorized licensed use limited to: The University of Osaka. Downloaded on April 23,2025 at 01:57:31 UTC from IEEE Xplore. Restrictions apply.

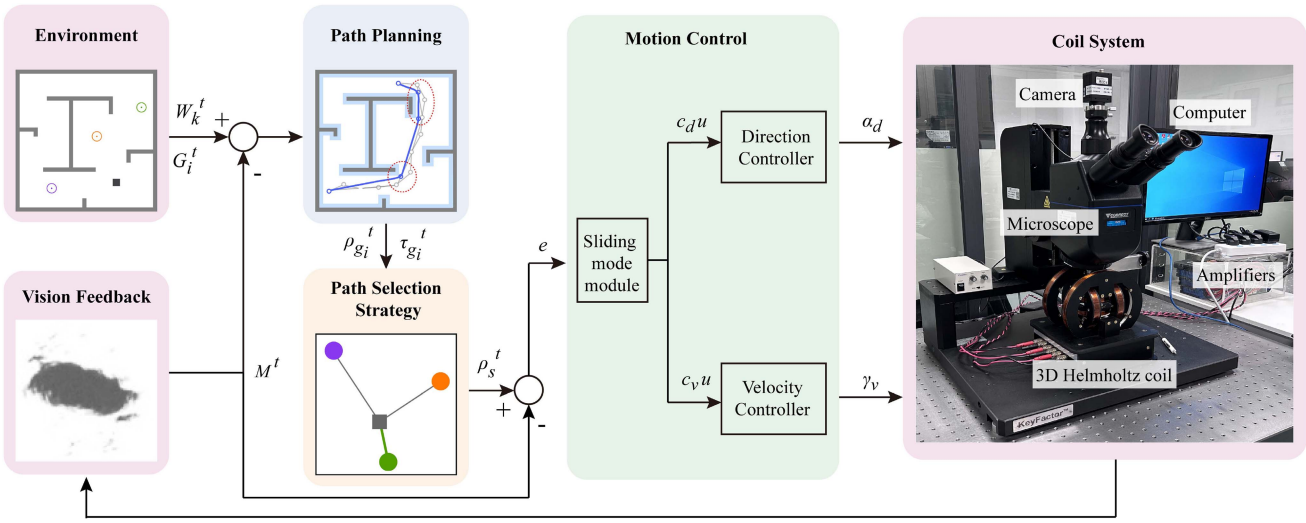

Fig. 4. The system diagram consisting of the ORRT* path planning unit, the path selection unit and the SM motion control unit. The positions of the swarm, the targets and the walls are represented by M^t, G_i^t and W_k^t, respectively. The planned paths and their lengths are denoted as $\rho_{g_i}^t$ and $\tau_{g_i}^t$. The shortest path is ρ_s^t and the distance error is e. The control signal of the sliding mode module is u. The desired direction angle and pitch angle are represented by α_d and γ_v.

the smaller value between m and n:

$$s(m,n) = \begin{cases} m, & m \le n \\ n, & m > n \end{cases} \tag{21}$$

The overall control scheme, which integrates the ORRT* path planner, the path selection strategy and the SM motion controller, is shown in Fig. 4. With a known environment, the positions of the targets $G^t_{i(i=1,2,\ldots,I)}$ and the walls of the micromaze $W^t_{k(k=1,2,\ldots,K)}$ can be obtained. The positions are input to the ORRT* path planner to generate desired paths $\rho^t_{g_{i(i=1,2,\ldots,I)}}$ connecting the swarm and the targets. Based on the lengths of the planned paths $\tau^t_{g_{i(i=1,2,\ldots,I)}}$, the path selection strategy chooses the shortest one and the immediate target is then obtained. The shortest planned path ρ_s^t serves as the input of the SM motion controller. Meanwhile, the position of the detected swarm M^t is regarded as the feedback signal of the path planner and the motion controller. The desired direction angle α_d and pitch angle γ_v are then obtained, which leads to the desired moving direction and velocity of the swarm.

III. Simulation

To validate the effectiveness of the control scheme, the simulation of multiple mobile targets tracking in a virtual micromaze is performed. The targets are designed as mobile circles, whose diameter and translational velocity are maintained as 208 μm and 16 μm/s, respectively. They are able to bounce when contacting with the walls of the micromaze. The simulated results are shown in Fig. 5. At the moment t_0, the ORRT* path planner can generate desired paths connecting the simulated swarm and three targets avoiding the collision with all maze walls. The path selection strategy picks the shortest path (i.e., the green curve) and Target 3 (i.e., the green circle) is then selected as the immediate target. The other two targets, with their paths marked as the gray curves, are neglected at the current stage.

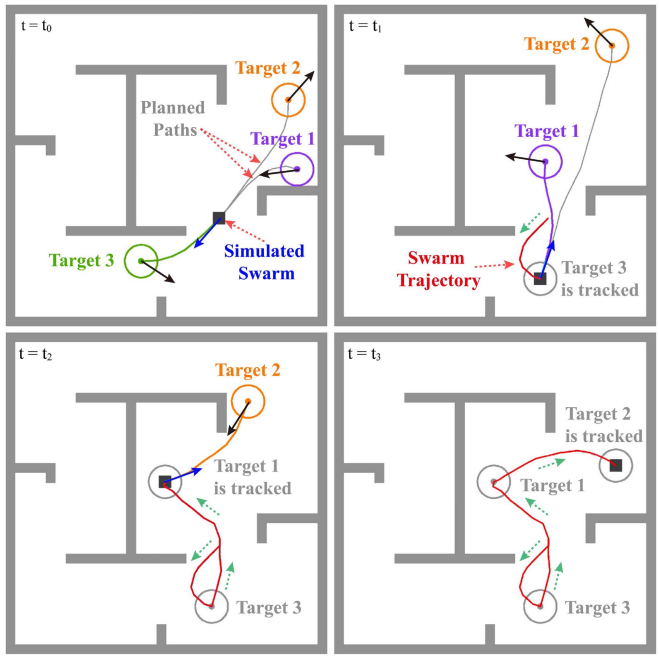

Fig. 5. The simulation results of tracking multiple mobile targets. The moving direction of the swarm and the target are represented by blue and black arrow, respectively. The colored curve is the shortest path, i.e., the path connecting the swarm and the immediate target, and the gray curves are the other planned paths. The red curve shows the trajectory of the swarm and the dotted green arrows show the moving direction of the simulated swarm.

The swarm is continuously navigated to follow the green path, and Target 3 is successfully tracked at moment t_1. The tracked target is deactivated and stopped afterwards, and is labelled with gray color. It is noted that, the moving directions of Target 1 and Target 2 have encountered sudden shifts due to the bouncing with the walls of the micromaze, but the ORRT* algorithm can still

Authorized licensed use limited to: The University of Osaka. Downloaded on April 23,2025 at 01:57:31 UTC from IEEE Xplore. Restrictions apply.

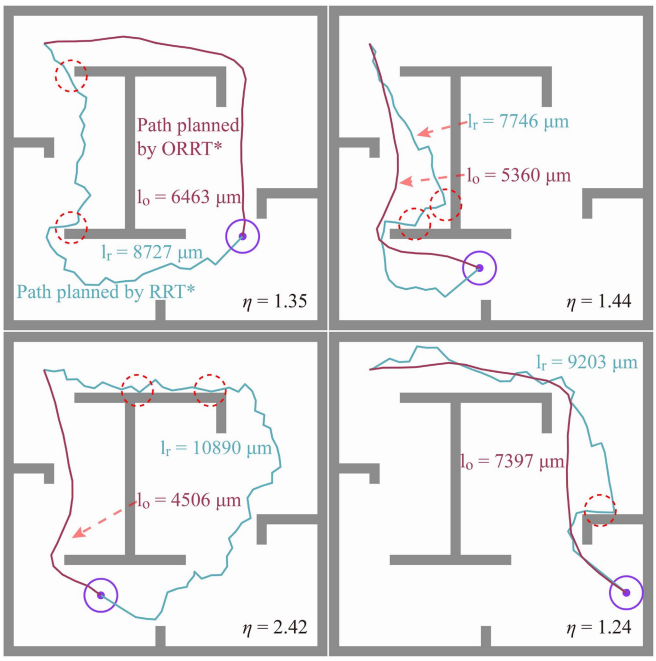

Fig. 6. The path lengths generated by different path planning algorithms in a micromaze. The brown curve shows the path generated by the ORRT* and its length is represented by l_o. The cyan curve represents the path generated by the basic RRT* and l_r denotes its length. The ratio between l_r and l_o is labelled by η. The red dotted circles indicate the regions of the collision between the swarm and walls of the micromaze.

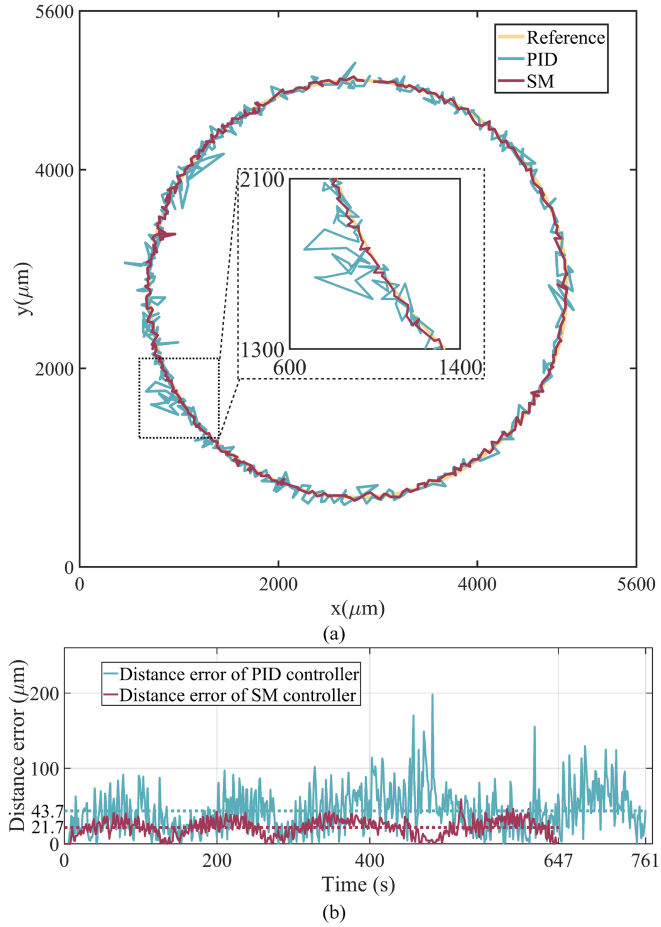

Fig. 7. The experimental results of path following of a microswarm in a free space with different motion controllers, i.e., the SM and PID motion controller. (a) The tracking results of path following. (b) The distance errors of the swarm. The average distance errors using SM and PID motion controller are 21.7 μm and 43.7 μm.

generate effective paths connecting the swarm and the targets. The swarm then follows the purple path, and Target 1 is tracked at moment t_2. Finally, the swarm follows the path connecting the swarm and Target 2 (i.e., the orange path), and Target 2 is tracked at moment t_3. Herein, all three targets are tracked. The simulation reveals that the proposed control scheme is effective for tracking multiple mobile targets in a highly constrained environment.

IV. Experimental Results

A. System Setup

A three-axial Helmholtz electromagnetic coil system, which consists of an optical microscope (Model PS888, SEIWA Optical CO., LTD.), an sCMOS camera (Model GS3-U3-41C6C-C, Teledyne FLIR LLC.) and a PC, is developed for experimental validation. The control signals are generated by the PC, and then the current is amplified into the coils to generate on-demand magnetic fields. The strength and frequency of the magnetic fields are maintained as 10 mT and 10 Hz, and the framerate of the camera is 10 frame per second (fps).

B. Validation of Path Planning Algorithm

By comparing the performance of the ORRT* path planning algorithm with basic RRT* path planner, the results are shown in Fig. 6. The experimental conditions, i.e., the positions of the swarm and the target, and the locations of the walls, are maintained the same. Even though the moving direction of the mobile target may change due to the bounces, the ORRT* path planner with a sufficient updating frequency (i.e., 1.8–2.6 Hz) can still generate desired paths avoiding collision with walls of the micromaze, as shown by the brown curves in Fig. 6. Since the physical size of the swarm is not taken into consideration in the basic RRT* algorithm, there are no collision buffer layers surrounding the walls. It may cause collision between the swarm and the walls, which are labelled using the red dotted circles in Fig. 6. Meanwhile, the length of the path generated by the ORRT* algorithm (i.e., l_o) is significantly shorter than that generated by the RRT* algorithm (i.e., l_r). The ratio between l_r and l_o, i.e., $\eta = l_r/l_o$, ranges from 1.24 to 2.42, which is shown in Fig. 6. The results indicate that the ORRT* algorithm can provide a better path for the swarm to track avoiding collision with the walls.

C. Validation of Motion Control Algorithm

In order to validate the effectiveness and accuracy of the proposed SM motion control algorithm for path following in a free environment, the PID motion controller is applied for

Authorized licensed use limited to: The University of Osaka. Downloaded on April 23,2025 at 01:57:31 UTC from IEEE Xplore. Restrictions apply.

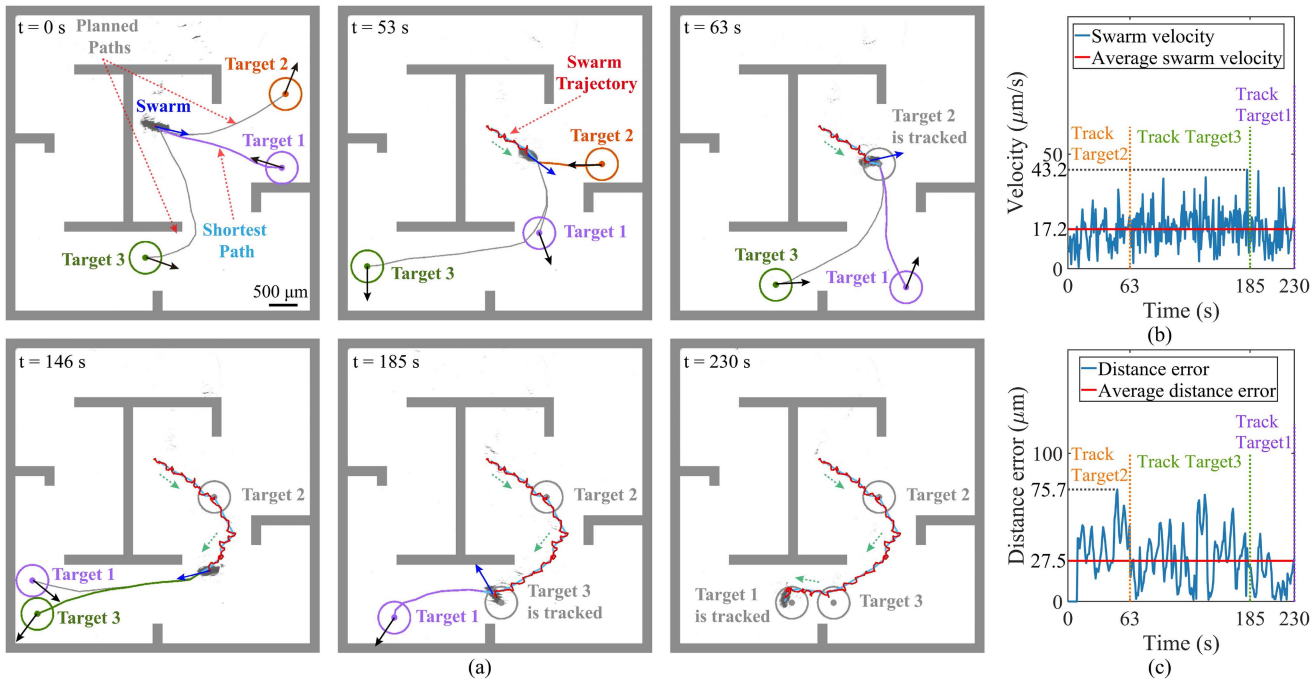

Fig. 8. The experimental results of tracking multiple mobile targets. (a) The trajectory tracking results of the swarm. (b) The velocity of the swarm. (c) The distance error of the swarm. The moving directions of the swarm and the targets are represented by blue and black arrows. The green dotted arrows show the moving direction of the swarm. The scale bar is 500 μm.

comparisons. The experimental results of controlling swarms to follow preset trajectories with the circular pattern are shown in Fig. 7(a). By observing the trajectory of the swarm, using the PID controller causes a relatively high distance error. However, the trajectory of the swarm using the SM controller well matches the reference path, indicating a small distance error. The curves of distance error e are presented in Fig. 7(b). When the SM controller is performed, the average distance error is 21.7 μm and the highest distance error is 66.9 μm. If the PID controller is applied, as shown in the green curve of Fig. 7(b), the average and highest distance error significantly increase to 43.7 μm and 234.7 μm, respectively. The results indicate that high accuracy of path following can be guaranteed using the SM motion controller.

D. The Tracking of Multiple Mobile Targets

In order to verify the effectiveness of the proposed control scheme, which combines the ORRT* path planning algorithm, the path selection strategy and the SM motion control algorithm, experiments of tracking multiple mobile targets in a virtual micromaze using a swarm are subsequently conducted. The circular bouncing targets, whose diameter and translational velocity are maintained as 208 μm and 16 μm/s, are applied. The experimental results are shown in Fig. 8. Since the path between the swarm and Target 1 (i.e., the purple path) is the shortest one among all three paths, Target 1 is selected as the immediate target for the swarm to track at $t = 0$ s. After several bouncing processes, the path between the swarm and Target 2 becomes the shortest one at $t = 53$ s, and the Target 2 is thus selected as the immediate target. The swarm is then controlled to track Target 2 by following the dynamically planned paths avoiding collision with walls of the micromaze. At $t = 63$ s, Target 2 is tracked by the swarm. At this moment, the swarm begins to track Target 1 because the path between them is the shortest. Due to the bouncing of the targets, the path between the swarm and Target 3 becomes the shortest one and the immediate target is replaced by Target 3 at $t = 146$ s. The swarm is subsequently controlled to track Target 3, which is achieved at $t = 185$ s. Finally, Target 1 is successfully tracked at $t = 230$ s. The experimental results have a good agreement with the simulation results shown in Fig. 5. From the results, the trajectory of the swarm (i.e., the red curve) well matches the planned path (i.e., the blue curve). The velocity and distance error of the swarm are shown in Fig. 8(b) and (c). The well controlled velocity ranging from 0 to 43.2 μm/s leads to a small average distance error (i.e., 27.5 μm), which is approximately 0.14 body length of the swarm. The oscillation amplitude of distance error in Fig. 8(c) maintains in a relatively small range (i.e., 0–75.7 μm). The results indicate that the SM controller can precisely control the moving direction and velocity of the swarm to guarantee the high tracking accuracy. As a result, the ORRT* path planner, the path selection strategy and the SM motion controller coordinate to achieve the accurate tracking of multiple mobile targets.

V. Conclusion

This work proposes an effective control scheme of the microswarm, which combines the ORRT* path planner, the path selection strategy and the SM motion controller, to track multiple

Authorized licensed use limited to: The University of Osaka. Downloaded on April 23,2025 at 01:57:31 UTC from IEEE Xplore. Restrictions apply.

mobile targets. The ORRT* path planning algorithm is developed to generate desired paths connecting the swarm and the targets in the constrained environments, i.e., the micromaze. The path selection strategy is then used to select the shortest path and determine the immediate target. The SM motion controller combines the sliding mode module, the direction controller and the velocity controller to guarantee the high tracking precision during the tracking process. By comparing with other methods, i.e., the RRT* path planner and the PID motion controller, the effectiveness of the ORRT* path planner and the SM motion controller are testified. Finally, simulations and experiments of tracking multiple mobile targets in a micromaze are conducted to further validate the robustness of the overall control scheme.

Since the proposed control scheme has a high compatibility, supplementary modules can be added to meet requirement of complicated conditions, e.g., a swarm moves on a curved surface or in an environment with fluid flows. The moving direction and the velocity of the swarm may be significantly affected by fluid flows in the environment. The proposed direction control algorithm can correct the deviation angle and the error of velocity can be compensated by adding a disturbance observer. The swarm velocity may be affected if the swarm moves on a curved surface. To maintain the distance error in a satisfactory range, tuning the pitch angle and adding a velocity adjustment module are potential approaches.

REFERENCES

[1] M. Sitti et al., "Biomedical applications of untethered mobile milli/microrobots," *Proc. IEEE*, vol. 103, no. 2, pp. 205–224, Feb. 2015.

[2] J. Li, E.-F de Ávila, B. Gao, W. Zhang, and J. Wang, "Micro/nanorobots for biomedicine: Delivery, surgery, sensing, and detoxification," *Sci. Robot.*, vol. 2, no. 4, 2017, Art. no. eaam6431.

[3] B. Ahmad, M. Gauthier, G. J. Laurent, and A. Bolopion, "Mobile microrobots for in vitro biomedical applications: A survey," *IEEE Trans. Robot.*, vol. 38, no. 1, pp. 646–663, Feb. 2022.

[4] M. Li, N. Xi, Y. Wang, and L. Liu, "Progress in nanorobotics for advancing biomedicine," *IEEE Trans. Biomed. Eng.*, vol. 68, no. 1, pp. 130–147, Jan. 2021.

[5] H. Zhou, C. C. Mayorga-Martinez, S. Pané, L. Zhang, and M. Pumera, "Magnetically driven micro and nanorobots," *Chem. Rev.*, vol. 121, no. 8, pp. 4999–5041, 2021.

[6] Y. Hu, "Self-assembly of DNA molecules: Towards DNA nanorobots for biomedical applications," *Cyborg Bionic Syst.*, vol. 2021, 2021, Art. no. 9807520.

[7] H. Lu et al., "A bioinspired multilegged soft millirobot that functions in both dry and wet conditions," *Nat. Commun.*, vol. 9, no. 1, pp. 1–7, 2018.

[8] H. Lu, Y. Hong, Y. Yang, Z. Yang, and Y. Shen, "Battery-less soft millirobot that can move, sense, and communicate remotely by coupling the magnetic and piezoelectric effects," *Adv. Sci.*, vol. 7, no. 13, 2020, Art. no. 2000069.

[9] R. Tan et al., "Nanofiber-based biodegradable millirobot with controllable anchoring and adaptive stepwise release functions," *Matter*, vol. 5, no. 4, pp. 1277–1295, 2022.

[10] R. H. Soon et al., "On-demand anchoring of wireless soft miniature robots on soft surfaces," *Proc. Nat. Acad. Sci.*, vol. 119, no. 34, 2022, Art. no. e2207767119.

[11] M. B. Akolpoglu et al., "Magnetically steerable bacterial microrobots moving in 3D biological matrices for stimuli-responsive cargo delivery," *Sci. Adv.*, vol. 8, no. 28, 2022, Art. no. eabo6163.

[12] Z. Ren, W. Hu, X. Dong, and M. Sitti, "Multi-functional soft-bodied jellyfish-like swimming," *Nat. Commun.*, vol. 10, no. 1, pp. 1–12, 2019.

[13] Q. Ze et al., "Spinning-enabled wireless amphibious origami millirobot," *Nat. Commun.*, vol. 13, no. 1, pp. 1–9, 2022.

[14] S. Li et al., "Soft magnetic microrobot doped with porous silica for stability-enhanced multimodal locomotion in a nonideal environment," *ACS Appl. Mater. Interfaces*, vol. 14, no. 8, pp. 10856–10874, 2022.

[15] Z. Wu et al., "A swarm of slippery micropropellers penetrates the vitreous body of the eye," *Sci. Adv.*, vol. 4, no. 11, 2018, Art. no. eaat4388.

[16] A. Servant, F. Qiu, M. Mazza, K. Kostarelos, and B. J. Nelson, "Controlled in vivo swimming of a swarm of bacteria-like microrobotic flagella," *Adv. Mater.*, vol. 27, no. 19, pp. 2981–2988, 2015.

[17] N. Huang, L. J. Martínez, E. Jaquay, A. Nakano, and M. L. Povinelli, "Optical epitaxial growth of gold nanoparticle arrays," *Nano Lett.*, vol. 15, no. 9, pp. 5841–5845, 2015.

[18] T. Xu et al., "Reversible swarming and separation of self-propelled chemically powered nanomotors under acoustic fields," *J. Amer. Chem. Soc.*, vol. 137, no. 6, pp. 2163–2166, 2015.

[19] J. Yan, M. Han, J. Zhang, C. Xu, E. Luijten, and S. Granick, "Reconfiguring active particles by electrostatic imbalance," *Nat. Mater.*, vol. 15, no. 10, pp. 1095–1099, 2016.

[20] F. Ma, S. Wang, D. T. Wu, and N. Wu, "Electric-field–induced assembly and propulsion of chiral colloidal clusters," *Proc. Nat. Acad. Sci.*, vol. 112, no. 20, pp. 6307–6312, 2015.

[21] J. Yu, T. Xu, Z. Lu, C. I. Vong, and L. Zhang, "On-demand disassembly of paramagnetic nanoparticle chains for microrobotic cargo delivery," *IEEE Trans. Robot.*, vol. 33, no. 5, pp. 1213–1225, Oct. 2017.

[22] H. Xie et al., "Reconfigurable magnetic microrobot swarm: Multimode transformation, locomotion, and manipulation," *Sci. Robot.*, vol. 4, no. 28, 2019, Art. no. eaav8006.

[23] W. Gao, A. Pei, R. Dong, and J. Wang, "Catalytic iridium-based Janus micromotors powered by ultralow levels of chemical fuels," *J. Amer. Chem. Soc.*, vol. 136, no. 6, pp. 2276–2279, 2014.

[24] H. Wang, J. Kan, X. Zhang, C. Gu, and Z. Yang, "PT/CNT micronanorobots driven by glucose catalytic decomposition," *Cyborg Bionic Syst.*, vol. 2021, 2021, Art. no. 9876064.

[25] B. J. Nelson, I. K. Kaliakatsos, and J. J. Abbott, "Microrobots for minimally invasive medicine," *Annu. Rev. Biomed. Eng.*, vol. 12, pp. 55–85, 2010.

[26] A. K. A. Silva, E. L. Silva, E. Egito, and A. S. Carriço, "Safety concerns related to magnetic field exposure," *Radiat. Environ. Biophys.*, vol. 45, no. 4, pp. 245–252, 2006.

[27] J. J. Abbott, E. Diller, and A. J. Petruska, "Magnetic methods in robotics," *Annu. Rev. Control Robot. Auton. Syst.*, vol. 3, no. 1, pp. 57–90, 2020.

[28] M. Salehizadeh and E. D. Diller, "Path planning and tracking for an underactuated two-microrobot system," *IEEE Robot. Autom. Lett.*, vol. 6, no. 2, pp. 2674–2681, Apr. 2021.

[29] F. Ongaro et al., "Autonomous planning and control of soft untethered grippers in unstructured environments," *J. Micro-Bio Robot.*, vol. 12, no. 1, pp. 45–52, 2017.

[30] X. Dong and M. Sitti, "Planning spin-walking locomotion for automatic grasping of microobjects by an untethered magnetic microgripper," in *Proc. IEEE Int. Conf. Robot. Automat.*, 2017, pp. 6612–6618.

[31] T. Xu, C. Huang, Z. Lai, and X. Wu, "Independent control strategy of multiple magnetic flexible millirobots for position control and path following," *IEEE Trans. Robot.*, vol. 38, no. 5, pp. 2875–2887, Oct. 2022.

[32] T. Xu, Y. Guan, J. Liu, and X. Wu, "Image-based visual servoing of helical microswimmers for planar path following," *IEEE Trans. Autom. Sci. Eng.*, vol. 17, no. 1, pp. 325–333, Jan. 2020.

[33] S. Xu, J. Liu, C. Yang, X. Wu, and T. Xu, "A learning-based stable servo control strategy using broad learning system applied for microrobotic control," *IEEE Trans. Cybern.*, vol. 52, no. 12, pp. 13727–13737, Dec. 2022.

[34] T. Xu, Z. Hao, C. Huang, J. Yu, L. Zhang, and X. Wu, "Multimodal locomotion control of needle-like microrobots assembled by ferromagnetic nanoparticles," *IEEE/ASME Trans. Mechatron.*, vol. 27, no. 6, pp. 4327–4338, Dec. 2022.

[35] T. Xu, J. Liu, C. Huang, T. Sun, and X. Wu, "Discrete-time optimal control of miniature helical swimmers in horizontal plane," *IEEE Trans. Autom. Sci. Eng.*, vol. 19, no. 3, pp. 2267–2277, Jul. 2022.

[36] L. Yang, J. Yu, and L. Zhang, "Statistics-based automated control for a swarm of paramagnetic nanoparticles in 2-D space," *IEEE Trans. Robot.*, vol. 36, no. 1, pp. 254–270, Feb. 2020.

[37] J. Nasir et al., "RRT*-SMART: A rapid convergence implementation of RRT," *Int. J. Adv. Robot. Syst.*, vol. 10, no. 7, pp. 299–310, 2013.

[38] L. Yang, Q. Wang, and L. Zhang, "Model-free trajectory tracking control of two-particle magnetic microrobot," *IEEE Trans. Nanotechnol.*, vol. 17, no. 4, pp. 697–700, Jul. 2018.

Authorized licensed use limited to: The University of Osaka. Downloaded on April 23,2025 at 01:57:31 UTC from IEEE Xplore. Restrictions apply.